Supporting Information for Edge State Engineering of Graphene Nanoribbons

Xuelei Su, Zhijie Xue, Gang Li,* and Ping Yu*

School of Physical Science and Technology, ShanghaiTech University, 201210 Shanghai, China

E-mail: ligang@shanghaitech.edu.cn; yuping@shanghaitech.edu.cn

Content:

Sample preparation

The 10,10′-dibromo-9,9′-bianthryl (DBBA) and MnPc molecules were purchased from Sigma Adrich. Samples were prepared by evaporation DBBA molecules onto a Au(111) substrate then annealed to 433 K as a first step. Subsequently, MnPc molecules were deposited on the sample and annealed with linear polymer chains for the second step at 593 K. By using this procedure we can obtain a few number of free AGNRs fusing with single MnPc molecule.

STM and AFM measurements.

All the STM/AFM experiments if not specified were performed at 5K with commercial Createc LT-STM/qPlus AFM. The qPlus sensor with a resonance frequency of 30.4 KHz, the oscillation amplitude of 50 pm. $\mathrm{d}I/\mathrm{d}V$ measurements were performed with an internal lock-in amplifier which frequency is 273 Hz with amplitude of 5 mV. To prepare the CO functionalized tungsten tip, NaCl were deposited on the sample. After dosing CO, we picked up CO molecule from the NaCl island. For the constant-height AFM images, the tip-sample distance is decreased a few hundred of pm from the STM set point V = 300 mV, I = 0.1 nA.

DFT calculation

First-principle calculations were carried out within density functional theory (DFT)[1,2] as implemented in Vienna Ab initio Simulation Package (VASP).[3] The projector augmented wave pseudopotential[4] are employed, and the exchange-correlation energy was treated with the generalized gradient approximation of Perdew, Burke and Ernzerhof (PBE).[5] The spin-orbit coupling of electrons was not considered in our calculations. The cutoff energy of the plane-wave basis functions was set to be 400 eV. For the reciprocal-space integration we used the Gamma-centered Monkhorst-Pack special k-point method[6] with $1 \times 1 \times 1$ grid in structure relaxation and with $3 \times 3 \times 3$ grid in electronic self-consistent calculations. The vacuum space is set to more than 10Å in all three directions to minimize artificial

interactions between neighbouring slabs. The energy convergence criteria is set to be 1 meV/atom. The atomic positions were fully relaxed using the conjugate gradient algorithm until all interatomic forces were small than 0.01 eV/Å. To partially account for the electronic correlations of the Mn d electrons, Dudarev type DFT + U functional with U = 3 eV was employed in both self-consistent and partial density of states calculations. The site-resolved density of states was calculated with a Gaussian broadening of 20 meV.

The electronic structure of MnPc-AGNRs at 77 K.

The zigzag edge state of AGNR fusing with MnPc show a double peak/dip structure around the Fermi level. It can be viewed as a pair of occupied and unoccupied electronic states around the Fermi level or a Kondo resonance with a dip feature at the Fermi energy. As well known, one characteristic of the Kondo effect is a strong temperature induced broadening of the Kondo resonance.[7] The $\mathrm{d}I/\mathrm{d}V$ spectra of MnPc-AGNR measured at 5 K and 77 K are shown in Fig. S1. Consistent with previous studies, MnPc molecules show Kondo effect with a step feature at the Fermi level at 5K. From fitting its $\mathrm{d}I/\mathrm{d}V$ spectra with a Fano function,[8,9]

$$\frac{dI}{dV} = A\frac{(\epsilon + q)^2}{1 + \epsilon^2} + B \tag{1}$$

where $\epsilon = (eV - \epsilon_0)/\Gamma$ and $\Gamma \sim k_B T_K$, the half width of Kondo resonance Γ is extracted and Kondo temperatrue T_K is estimated as 49 K. Therefore, the Kondo resonance on MnPc vanishes at 77 K above the Kondo temperature. On the other hand, if the double peak/dip feature of the dI/dV spectrum measured at the zigzag edge fusing with MnPc is a Kondo effect, the origin of the Kondo effect of the zigzag edge is most likely due to the magnetic impurity of MnPc. In this case, its Kondo temperature should not be higher than MnPc Kondo temperature. However, if the dip feature is fitted with a Fano function, its Kondo temperature is derived as large as 156 K, which seems implausible. Moreover, the dip feature shows no Kondo temperature dependence. There is no dip any more but two broad peaks in

the dI/dV spectrum of the zigzag edge fusing with MnPc measured at 77 K. If we attribute the electronic states feature to two peaks rather than a dip and fit the two peaks with Gaussian functions for 5 K and 77 K respectively, the broadening of the peak width is found to result only from the thermal effect. Therefore, it is more plausible to recognize the electronic structure of zigzag edge fusing with MnPc as a pair of occupied and unoccupied electronic states rather than Kondo effect.

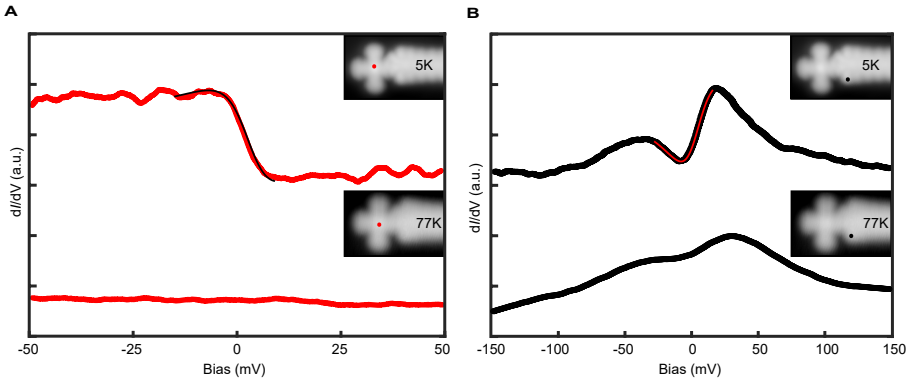

Figure S1: The electronic structure of MnPc-AGNRs measured at 5 K and 77 K. (A) $\mathrm{d}I/\mathrm{d}V$ spectra measured on the magnetic core of MnPc at 5 K and 77 K. (B) $\mathrm{d}I/\mathrm{d}V$ spectra measured on the zigzag edge of MnPc-AGNRs at 5 K and 77 K

$\mathrm{d}I/\mathrm{d}V$ spectra measured on the center of H-MnPc/MnPc.

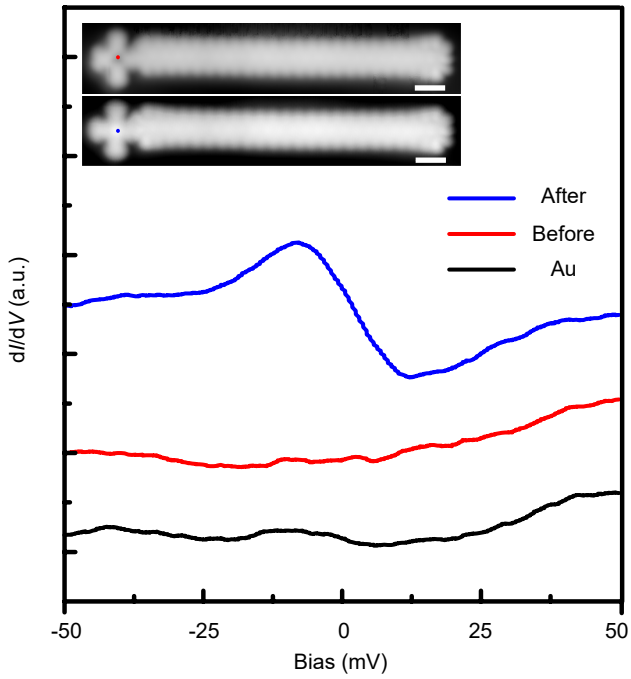

Figure S2: $\mathrm{d}I/\mathrm{d}V$ spectra measured on the center of H-MnPc/MnPc before and after applying a voltage pulse. Before voltage pulse, there is no electronic states near the Fermi level on the center of H-MnPc, while a sharp step appears near the zero bias voltage after pulsing.

Another example for engineering the ZES electronic structure of MnPc-AGNR.

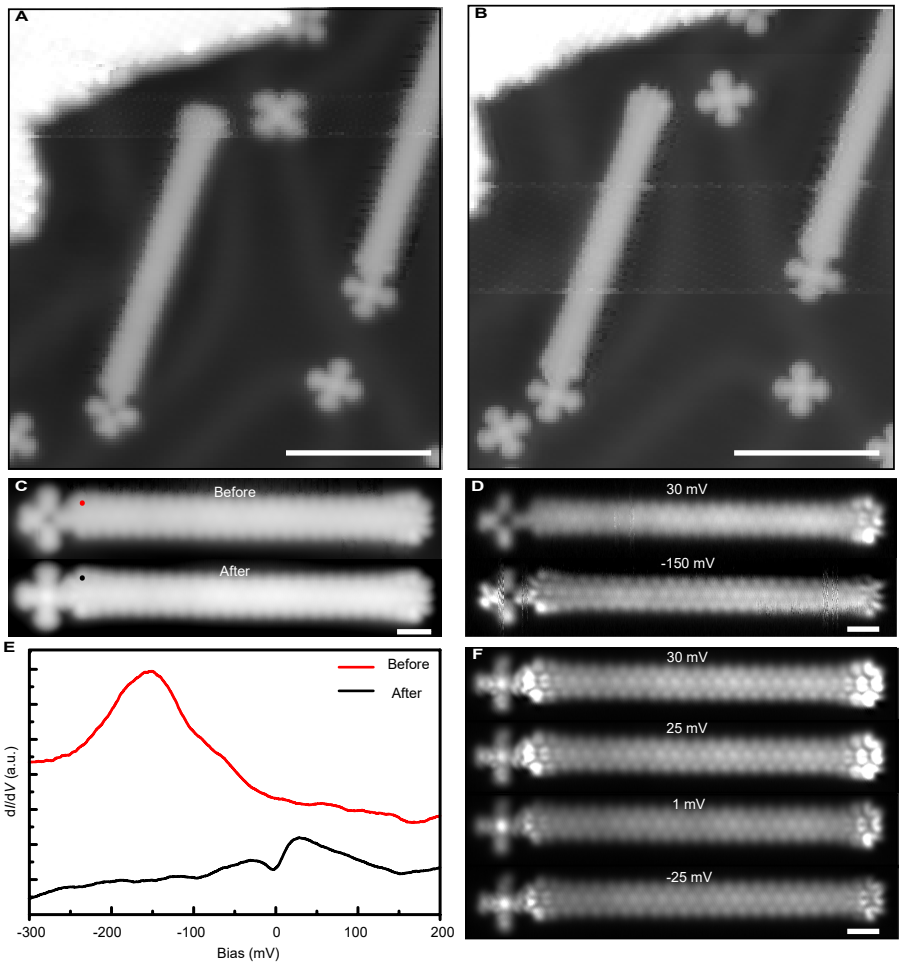

Figure S3: Engineering the ZES electronic structure. (A,B) STM overviews of H-MnPc/MnPc-AGNR before (A) and after (B) voltage pulsing. (C) High-resolution constant-current STM images before (up) and after (down) voltage pulsing. (D) Constant-height $\mathrm{d}I/\mathrm{d}V$ mappings measured at the bias voltages of 30 mV and -150 mV before pulsing. (E) $\mathrm{d}I/\mathrm{d}V$ spectra measured on top of the H-MnPc/MnPc-AGNR edge positions marked in (C). (F) Constant-height $\mathrm{d}I/\mathrm{d}V$ mappings measured at bias voltages of 30 mV, 25 mV, 1 mV, and -25 mV after pulsing. In (A), (B) scale bars, 5 nm, other scale bars, 1 nm.

dI/dV spectra measured across the H-MnPc-AGNR junction.

To investigate if the electronic state of -150 mV is the zigzag edge state of H-MnPc-AGNR or not, we have performed dI/dV spectra measured at different positions of MnPc as well as the connected AGNR for comparison, where are marked in Fig. S4A. The dI/dV mapping of -150 mV shown in Fig. S4B suggests that the electronic state of -150 mV show the highest electronic density at the zigzag edge of H-MnPc-AGNR. Moreover, the dI/dV spectra in Fig. S4C also represent that the intensity of the electronic state at -150 mV at the zigzag edge of H-MnPc-AGNR has the most pronounced intensity. Therefore, we attribute this -150 mV electronic state to the zigzag edge of H-MnPc-AGNR instead of the electronic state of H-MnPc molecule. (One benzene ring of H-MnPc in the dI/dV mapping of -150 mV in Fig. S3D shows strong intensity, which is due to the Au(111) reconstruction under this benzene ring. Without reconstruction influence, the most pronounced density of state at -150 mV is located at the zigzag edge of H-MnPc-AGNR).

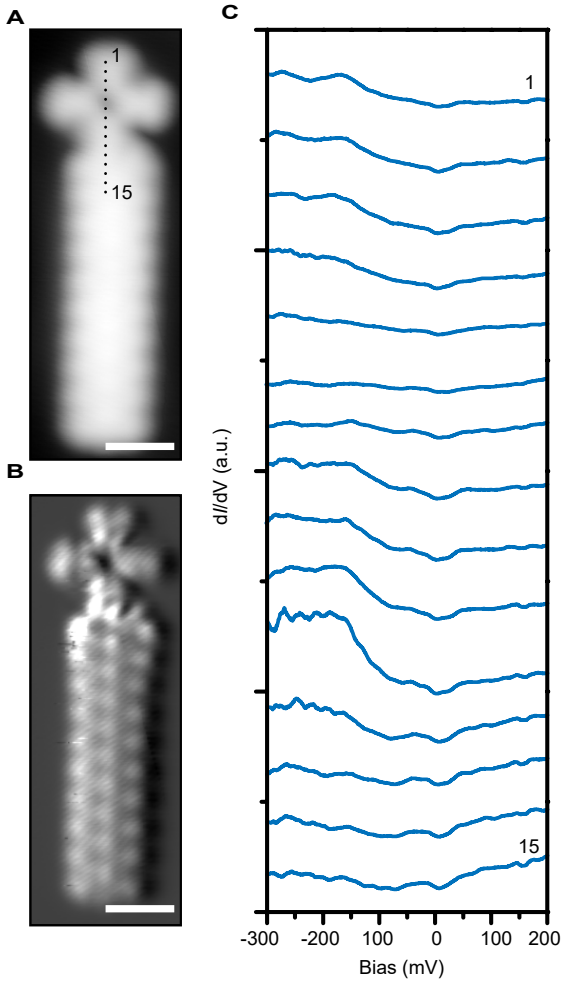

Figure S4: $\mathrm{d}I/\mathrm{d}V$ spectra measured across the H-MnPc-AGNR junction. (A) STM image of H-MnPc-AGNR. (B) Constant-height $\mathrm{d}I/\mathrm{d}V$ mappings measured at the bias voltages of -150 mV. (C) $\mathrm{d}I/\mathrm{d}V$ spectra measured at the positions of 1-15 on H-MnP-AGNR as marked in (A). Scale bars, 1 nm.

KPFS measurements

We have performed the Kelvin probe force spectroscopy (KPFS) measurements along the H-MnPc-AGNR and MnPc-AGNR respectively. For each KPFS, the frequency shift f (V) was recorded as a function of sample voltage V . From fitting f(V) as a function of sample voltage V to a parabola, the voltage at maximum value of f (V) is extracted, which is equal to the local contact potential difference (LCPD) between tip and sample. The representative KPFS measured on the Au(111) substrate and the zigzag edges are shown in Fig. S5.

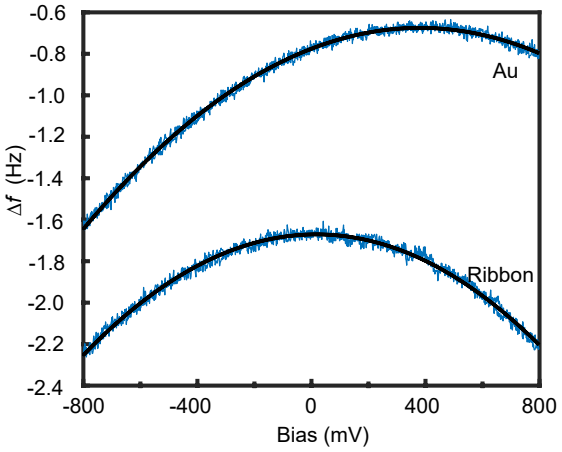

Figure S5: Representative KPFS measured on Au(111) substrate and on the zigzag edge of H-MnPc-AGNR.

Band gap of the ANGRs

The band gap of the investigated ANGRs is about 2.2 eV as shown in Fig. S6, which agrees well with the previous study.[10]

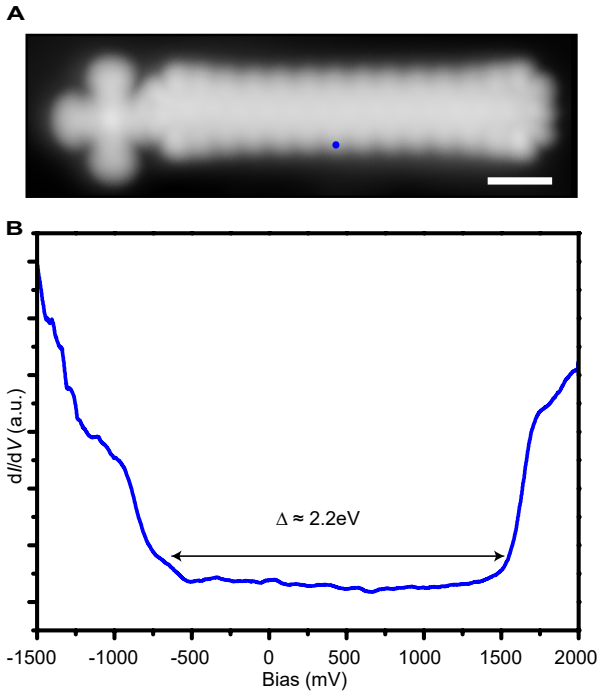

Figure S6: Representative band gap measurement on the investigated AGNRs.

Electronic structure of the edge states on the MnPc-AGNRs with different ribbon lengths

As the Fig. S7 shown below, the electronic states of two zigzag edges were measured on the different ribbon lengths. The electronic structure of the two zigzag edges are not affected by tuning the graphene nanoribbon length, which all show that a single peak above the Fermi level at the bare zigzag edge and two splitting peaks at the zigzag edge with MnPc fusing. In our experiments, the electronic structure of the zigzag edge is mostly dependent on the charging state of the zigzag edge. If the zigzag edge is neutral, the energy splitting should be observed as theoretical calculations predicted. Once the zigzag edge is positively charged, only one unoccupied edge state can be detected above the Fermi level, while when the zigzag edge is negatively charged, only the occupied edge state can be detected below the Fermi level. Therefore, in our experimental results the electronic structure of the edge state engineered by MnPc fusing is independent on the length of the investigated AGNRs.

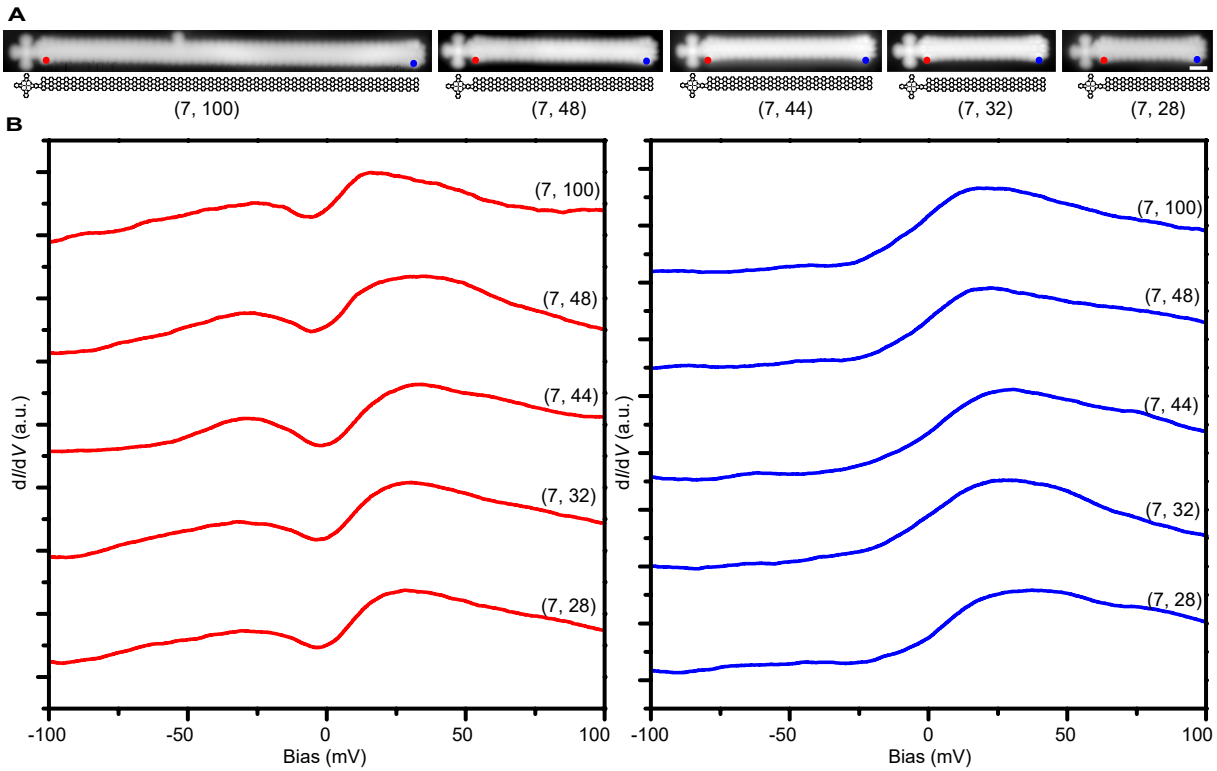

Figure S7: $\mathrm{d}I/\mathrm{d}V$ spectra measured on the MnPc-AGNRs zigzag edges with different ribbon lengths. Indices (m, n) are used to denote the number of carbon atoms of a graphene nanoribbon (GNR) along the zigzag (m) and armchair direction (n), respectively.

Density of states of carbon atoms at the far edges of MnPc-AGNRs

In Fig. S8 we show the corresponding density of states for the carbon atom locating at the far edge. By comparing all four plots, one clearly see that the edge states of the opposite far zigzag edges of MnPc-AGNRs are the same as the zigzag edge of free AGNR, indicating that the electronic structure of the far zigzag edge is not influenced by the two edges interaction. Nevertheless, the opposite two zigzag edges have magnetic correlation. As shown in the isovalued spin density surface overlaying on the structure model, the spins on the two zigzag edges prefer antiferromagnetic alignment, which agrees with the previous theoretical calculations.[11–14] However, the tip used in our experiments is not spin polarized. Therefore, the spin-resolved electronic states and the magnetic coupling effect as predicted by the theoretical calculation results can not be addressed in our work. Actually, as far as we know, there is still no conclusive experimental evidence to clearly show the zigzag edge state is spin polarized. In principle, the spin polarization of the zigzag edges may be resolved by using spin-polarized tunneling from a magnetic tip. These challenging spin resolved experiments can be further investigated in the future.

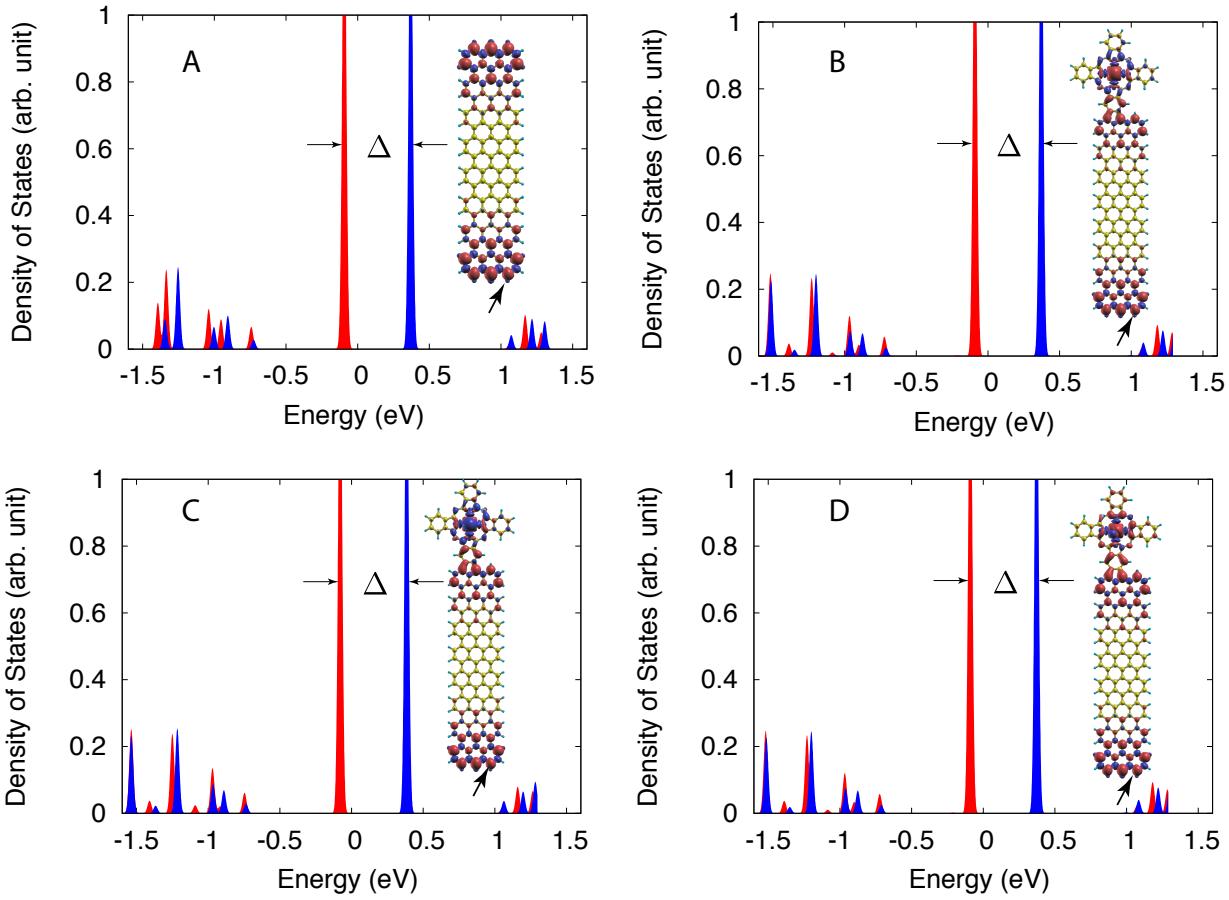

Figure S8: The density of states of carbon atom at the far edges of the MnPc-AGNRs indicated by the arrow in the inset structure model. (A-D) correspond to the AGNR, MnPc-AGNR, H-MnPc-AGNR and H2-MnPc-AGNR, correspondingly. The spin-polarized local density of states of chosen carbon atom is shown in red and blue colors corresponding to the minority and majority components. The inset shows the fully relaxed structure model and the overlaying isovalued spin density surface with red and blue colors denoting the minority and majority of spin directions.

References

(1) Hohenberg, P. & Kohn, W. Inhomogeneous electron gas. *Phys. Rev.* **136**, B864–B871 (1964).

(2) Kohn, W. & Sham, L. J. Self-consistent equations including exchange and correlation effects. *Phys. Rev.* **140**, A1133–A1138 (1965).

(3) Kresse, G. & Furthmüller, J. Efficient iterative schemes for ab initio total-energy calculations using a plane-wave basis set. *Phys. Rev. B* **54**, 11169 (1996).

(4) Blöchl, P. E. Projector augmented-wave method. *Phys. Rev. B* **50**, 17953–17979 (1994).

(5) Perdew, J. P., Burke, K. & Ernzerhof, M. Generalized gradient approximation made simple. *Phys. Rev. Lett.* **77**, 3865 (1996).

(6) Monkhorst, H. J. & Pack, J. D. Special points for brillouin-zone integrations. *Phys. Rev. B* **13**, 5188–5192 (1976).

(7) Nagaoka, K., Jamneala, T., Grobis, M. & Crommie, M. Temperature dependence of a single kondo impurity. *Physical Review Letters* **88**, 077205 (2002).

(8) Fano, U. U. fano, phys. rev. 124, 1866 (1961). *Phys. Rev.* **124**, 1866 (1961).

(9) Hofstetter, W., König, J. & Schoeller, H. Kondo correlations and the fano effect in closed aharonov-bohm interferometers. *Physical Review Letters* **87**, 156803 (2001).

(10) Ruffieux, P., Cai, J., Plumb, N. C., Patthey, L., Prezzi, D., Ferretti, A., Molinari, E., Feng, X., Müllen, K., Pignedoli, C. A., & Fasel, R. Electronic structure of atomically precise graphene nanoribbons. *ACS Nano* **6**, 6930–6935 (2012).

(11) Nakada, K., Fujita, M., Dresselhaus, G & Dresselhaus, M. S. Edge state in graphene ribbons: Nanometer size effect and edge shape dependence. *Physical Review B* **54**, 17954–17961 (1996).

(12) Yang, L., Park, C.-H., Son, Y.-W, Cohen, M. L. & Louie, S. G. Quasiparticle energies and band gaps in graphene nanoribbons. *Physical Review Letters* **99**, 186801 (2007).

(13) Yazyev, O. V. Emergence of magnetism in graphene materials and nanostructures. *Reports on Progress in Physics* **73**, 056501 (2010).

(14) Golor, M., Koop, C., Lang, T. C., Wessel, S. & Schmidt, M. J. Magnetic correlations in short and narrow graphene armchair nanoribbons. *Physical Review Letters* **111**, 085504 (2013).